Brillouin spectroscopy of biorelevant fluids in relation to viscosity and solute concentration

S. V. Adichtchev,[1] Yu. A. Karpegina,[1] K. A. Okotrub,[1] M. A. Surovtseva,[2] V. A. Zykova,[1] and N. V. Surovtsev[1,*]

[1]*Institute of Automation and Electrometry, Russian Academy of Sciences, Novosibirsk 630090, Russia*

[2]*Research Institute of Clinical and Experimental Lymphology—Branch of Institute of Cytology and Genetics, Russian Academy of Sciences, 630060 Novosibirsk, Russia*

(Received 13 February 2019; revised manuscript received 18 April 2019; published 18 June 2019)

The measurement of intracellular viscoelastic properties by Brillouin scattering is a rapidly developing field in biophysics and medicine. Here, the Brillouin spectroscopy is applied for a number of aqueous solutions of biorelevant molecules to reveal relations between the Brillouin line parameters (frequency and width) and viscosity or solute concentration. It is found that for the majority of the studied biorelevant molecules the solute concentration governs the Brillouin frequency in a universal manner. On the other hand, the relations between the macroscopic viscosity and Brillouin peak parameters are different for different solutes. We conclude that for biological fluids the viscosity evaluation from Brillouin data needs prior knowledge about the chemical composition. This result challenges the fidelity of the indirect experimental determinations of the cellular viscosity, when small molecule solutions are used for the calibration.

DOI: 10.1103/PhysRevE.99.062410

I. INTRODUCTION

Mechanical properties of cells and tissues are considered as an important factor for description of the morphological structures, for developmental and pathological processes, for improving the medical diagnostics, and for the regulating biomechanics. In this direction, one of the hot topics is the study of the viscoelastic properties of living cells by Brillouin spectroscopy [1–6]. Brillouin spectroscopy has advantages of label-free, noncontact and noninvasive optical techniques, which can be realized in a microscopical variant providing a distribution of the elastic parameters with micrometer spatial resolution. Recent progress in Brillouin spectrometers [7–9] opens doors to various biological and medical applications of Brillouin spectroscopy [10–19].

Brillouin scattering is inelastic light scattering with generation or absorption of acoustic phonons. Brillouin spectra consist of peaks shifted on frequencies $\pm\nu_b$ relative to the excitation light frequency. The frequency shift is defined by the relation

$$\nu_b = \frac{2n}{\lambda} u \sin\left(\frac{\theta}{2}\right), \tag{1}$$

where λ is the excitation wavelength in vacuum, n is the refractive index, θ is the scattering angle, and u is the acoustic velocity. Thus, the Brillouin line frequency provides values of the acoustic velocity and through the relation $M(\nu_b) = \rho u^2$ about the adiabatic elastic modulus. There are two contributions to the Brillouin linewidth. One is inhomogeneous broadening due to the distribution of ν_b, and the second is homogeneous broadening caused by the finite phonon lifetime due to dissipative processes. In the case of the negligible inhomogeneous broadening the full width at half maximum Γ_b of the Brillouin line is related to the viscosity η via [20]

$$\eta(\nu_b) \propto \Gamma_b/\nu_b^2. \tag{2}$$

For the excitation light in visible range, the Brillouin lines are within the GHz range. Thus, the Brillouin spectroscopy is widely used to find the sound velocities, the elastic modulus, and the apparent viscosity $\eta(\nu_b)$ in various materials.

It is believed this light scattering technique can characterize the elastic modulus and apparent viscosity of cells with submicrometric resolution. On the other side, intracellular content can be considered as a fluid, and those properties at fixed external conditions should be determined by the chemical composition. Usually, water contribution dominates in cell cytoplasm composition (from 80% by weight or more). From a naive view, the intracellular content can be considered as an aqueous solution or suspension. Indeed, Brillouin line frequency in previous studies of cells [1–6] is much closer to the case of water (~7.5 GHz for the green light and backscattering geometry) than to solid organics (typically, 15–20 GHz). Therefore, for this paper, we can define a term "biorelevant solution" as an aqueous solution of the bio-organic substances that can be found in cell cytoplasm (proteins, saccharides, amino acids, etc.) at concentrations near physiological.

Application of Brillouin spectroscopy in the studies of biospecimens raises important questions underpinning the interpretation of Brillouin experiment outcomes: What is the relation between the GHz elastic modulus of cellular fluids and the solute concentration? How does this relation depend on the particular solute? What is the relation between the Brillouin line frequency and linewidth and the zero-frequency viscosity of the cellular fluids? In the present work, we found answers to these questions by studying the Brillouin spectra of the aqueous solutions of the biorelevant molecules and cell cytosol.

*lab21@iae.nsk.su

II. EXPERIMENT

A. Samples

Aqueous solutions of different weight concentration were prepared from distilled water and different substances of chemical grade: glycine (up to 20 wt %), triglycine (up to 10 wt %), sucrose (up to 60 wt %), glycerol (up to 100 wt %), lysozyme (up to 40 wt %), and bovine serum albumin (BSA, up to 30 wt %). Solutions of food gelatin were prepared from a common source (up to 5 wt %). Also, samples from egg white were prepared; to vary those weight fractions some of them were dried or wetted.

A sample of a cell cytosol was prepared from a culture of rat mesenchymal stem cells. Cultured cells were collected and precipitated by centrifugation (1500 *g*, 10 min). The supernatant was removed and the cell pellet exposed to two freeze (−195 °C) and thaw (37 °C) cycles followed by centrifugation (470 *g*, 15 min). The supernatant of this centrifugation was collected and centrifuged at 15 000 *g* for 20 min. The resulting supernatant (0.25 ml) contained the cytoplasm without cytoplasmic membranes and ribosomes. Raman spectra did not reveal the notable contribution of the symmetric CH_2 stretching vibrations, which are an indicator of lipids (and, vice versa, this contribution was very notable for the sediment after centrifugation). Thus, the contribution of the cytoplasmic membranes is low in the sample, which can be considered as a representative for the cell cytosol.

The viscosity of the samples was measured by the custom-made capillary viscometer, which allows providing measurement with a small sample volume (∼150 μL). The viscometer was calibrated by comparison with literature data for aqueous glycerol solutions. For the Brillouin experiment, the samples were placed in glass ampoules and sealed by paraffin.

B. Brillouin experiment

The unpolarized Brillouin spectra were collected in backscattering geometry with a 3+3-pass Sandercock tandem Fabry-Perot interferometer. Brillouin scattering was excited by a laser with wavelength 532.1 nm. The free spectral range was 20 GHz and the finesse was 100. The spectral resolution was determined by measuring the elastically scattered line, which had a 0.2-GHz width (Gaussian contour was used for the description). The experiment was carried out at room temperature, which was 296 ± 1 K.

III. RESULTS AND DISCUSSION

The Brillouin spectra of aqueous glycerol of representative concentrations are shown in Fig. 1. Sharp peaks in the Stokes and anti-Stokes side correspond to the inelastic light scattering with generation or absorption of the longitudinal acoustic waves. Spectra of other fluids look similar. Addition of the nonaqueous component to the fluid increases the Brillouin line frequency and linewidth (Fig. 1). The Brillouin line frequency was determined as the frequency of the peak maximum. Estimated error in the Brillouin line frequency did not exceed 0.08 GHz. To evaluate the true width of the Brillouin line, the experimental line was described by a Voigt contour, which takes into account the instrumental resolution, as the Gaussian

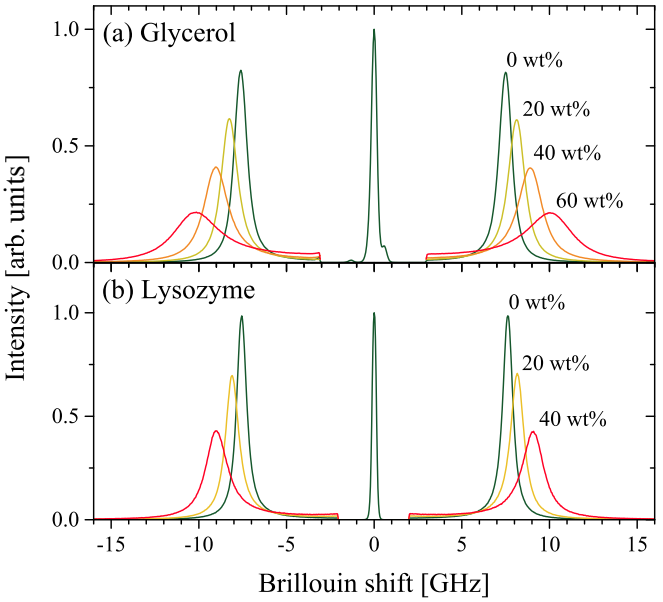

FIG. 1. Brillouin spectra of aqueous glycerol (a) and lysozyme (b) solutions for representative solute concentrations. Elastic line (at zero frequency) comes from the reference beam [21].

contour with a width of 0.2 GHz. Estimated error in the evaluated linewidths was ∼0.05 GHz.

In Fig. 2 the Brillouin line frequencies and linewidths, corrected by the instrumental resolution, are shown for the aqueous solution of different substances. The line frequency demonstrates a universal dependence on the mass fraction for the most biorelevant substances. This universal dependence works up to about 40 wt %. The Brillouin peaks of glycerol and sucrose (those solutions can be prepared for higher concentrations) have different frequencies at the concentration above 40 wt %. The linewidths of the different biorelevant fluids show the same increase with the solute concentration up to ∼20 wt %.

The universality of the Brillouin line frequency versus mass fraction for the majority of the samples studied invites a chemical substance-free explanation. Let us apply formally a biphasic model to an aqueous solution in which one phase is water and the second phase is a solute. This implies that some elastic modulus M_S is attributed to the solutes. In the case of the same stress conditions, the effective elastic modulus of the solution M_{eff} is written [23] as

$$\frac{1}{M_{\text{eff}}} = \frac{1-x}{M_W} + \frac{x}{M_S}, \tag{3}$$

where M_W is the elastic modulus of water and x is the solute volume fraction. For simplicity, we neglect the changes in the refractive index with concentration growth and in the solution density (in a first approximation these corrections correlate with x and should be close for different solutes). In this case, Eq. (3) provides the prediction for the Brillouin line frequency of the solution ν_b^{eff}:

$$\nu_b^{\text{eff}} = \frac{\nu_b^W}{\sqrt{1-x+xu_W^2/u_S^2}}, \tag{4}$$

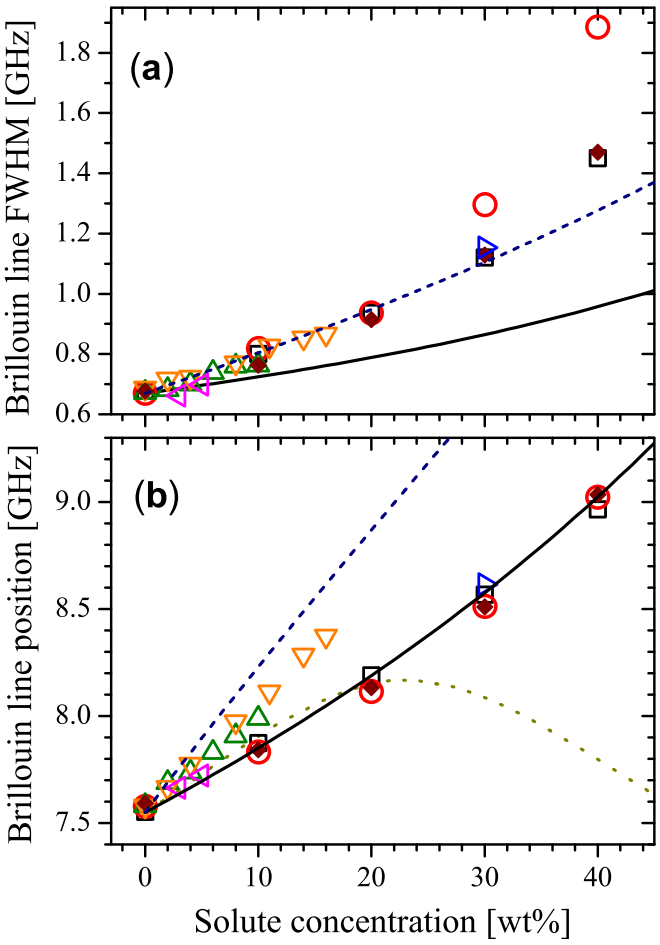

FIG. 2. Brillouin linewidth (a) and line frequency (b) of the biorelevant aqueous solutions versus solute concentration of non-aqueous components: glycine (down triangles), triglycine (up triangles), glycerol (squares), sucrose (circles), lysozyme (diamonds), BSA (right triangles), gelatin (left triangles). The solid lines are predictions from Eq. (5) for (a) and Eq. (4) for (b). The dashed line in (a) is a fit from Eq. (6); in (b) it is an average between Eqs. (4) and (8) predictions. The dotted line in (b) corresponds to the aqueous solution of ethanol according to the sound velocities reported in [22].

where ν_b^W is the Brillouin line frequency of water; u_W and u_S are the sound velocities of water and solute, respectively. In the assumption that all biorelevant substances provide approximately the same sound velocity, Eq. (4) predicts the Brillouin line frequency versus the solute concentration. The line in Fig. 2(b) shows the prediction for $u_W = 1.5$ km/s and $u_S = 3$ km/s (this value is a reasonable estimation for solid organic, e.g., sound velocity of polymethylmethacrylate ~2.8 km/s, lysozyme crystal varies from ~2.7 to 3.2 km/s). It is seen that Eq. (4) works exceptionally well for most solutions in Fig. 2(b).

The proposed model is oversimplified to reveal the main reason for the universality of the relation between the Brillouin line frequency and mass fraction for biorelevant fluids, found in the present work. A minimal number of material parameters is involved in Eq. (4). It can be shown (see the Appendix) that the proposed biphasic description of experimental results works similarly when changes in density and refraction are taken into account.

The Brillouin linewidth Γ relates to the relaxation susceptibility $\chi''(\nu)$ via $\Gamma \propto \nu\chi''(\nu)$. Since the water relaxation susceptibility is approximately proportional to the frequency in the GHz range (the water relaxational maximum takes place at 90 GHz [24]), then for the unchanged $\chi''(\nu)$ the Brillouin line width depends on the Brillouin shift as:

$$\Gamma(\nu_b) \propto \nu_b^2. \tag{5}$$

It is seen that the effect of Eq. (5) is not enough to account the concentration-related changes in Γ. There is an additional broadening, which should be associated with some changes in $\chi''(\nu)$. On the other hand, these changes should be similar for different solutes [Fig. 2(a)]. A simple interpretation can be suggested, where changes in $\chi''(\nu)$ are associated with the increase of the hydration water molecules [25]. For low concentration the solute-related increase of the $\chi''(\nu = \nu_b)$ is proportional to x, so

$$\Gamma(\nu_b) \propto \nu_b^2 + \alpha x. \tag{6}$$

In the simplest approximation, that the hydration number per solute mass is the same for biorelevant solutes studied (this implies the same ratio between the effective hydrophilic surface of a molecule and its mass), then Eq. (6) should describe $\Gamma(x)$ of all solutions with the same α. In Fig. 2(a) it is seen that this expectation works well up to ~20 wt % for the biorelevant solutes studied.

The Brillouin line frequency in the case of glycine and triglycine demonstrates the significant deviation from the common dependency in Fig. 2(b). We attribute this to their specific interaction with water structure. Molecules of these substances include hydrophobic parts and are less soluble in water in comparison with other substances in our study. Probably, glycine and triglycine have more extended effects on water structure, and the assumption of the same stress conditions, Eq. (3), is not so good. In the case of the same deformation conditions within the biphasic model, M_{eff} is [23]

$$M_{\text{eff}} = (1 - x)M_W + xM_S, \tag{7}$$

so

$$\nu_b^{\text{eff}} = \nu_b^W \sqrt{1 - x + xu_S^2/u_W^2} \tag{8}$$

[the same simplification as for Eqs. (3) and (4)]. The case of two interpenetrating extended phases being a compromise between Eqs. (4) and (8) can be expected. The dashed line in Fig. 2(b) corresponds to the average between ν_b^{eff} predicted by Eqs. (4) and (8). It is seen that the values for glycine and triglycine are not far from this line. Thus, probably, the specificity of these substances in Fig. 2(b) is related to their specific effect on water structure, which limits the applicability of Eq. (4).

Figure 2 evidences that in many cases the variations of the Brillouin line parameters, observed in biorelevant fluid or cellular components, provide not only elastic modulus and GHz viscosity but also the solute concentration. Namely, the

nonaqueous component concentration is the governing parameter of the GHz elastic response of biorelevant fluids. Very recently, it was shown [26] that the Brillouin frequency of the hydrogels is determined by solute concentration up to about 8 wt % of the solute; also Eq. (3) was applied to explain the findings of this work. Our results in Fig. 2 show that this can be true for aqueous fluids of many solutes with concentration up to 40 wt %. Also, the universal behavior is found for $\Gamma(x)$. These outcomes provide a simple interpretation of the Brillouin results in cellular components and in tissues with a high water concentration.

In the case of the aqueous solution of a liquid with the sound velocity lower than that for water (e.g., ethanol), the dependence of the Brillouin line frequency versus concentration should describe the transition from the water's Brillouin line frequency to a lower value. However, from the above oversimplified reasoning [Eqs. (3) and (4)], one can expect that instead of a monotonic decrease of the Brillouin line frequency versus the solute concentration some increase should be observed at low concentrations. Indeed, the nonmonotonic concentration dependence of the sound velocity is known for ethanol [22]. In Fig. 2(b) we adapted the sound velocity of an aqueous ethanol solution (from [22]) to calculate the expected Brillouin line frequencies. It is seen that up to approximately 20 wt % this dependence surprisingly well follows the main tendency and is described by Eq. (4).

We also checked whether there is a simple relation between the macroscopic (zero-frequency) viscosity and the Brillouin line parameters. It was found that there is no simple relation between the Brillouin parameters and the viscosity, which could be applied without knowledge about the composition of a fluid. For example, 5 wt % of gelatin increases the solution viscosity 18 times, while the Brillouin line parameters change slightly (Fig. 2). In contrast, 16 wt % of glycine changes the Brillouin line parameters more strongly (Fig. 2), whereas the solution viscosity is increased only 1.3 times. Figure 3 demonstrates the interrelations between the Brillouin line parameters and the viscosity for the fluids studied. In this image, data with viscosity up to ~7 cP are considered to show in detail the viscosity range relevant for the cellular components.

Figure 3 shows that fluids of different composition form different branches of the Brillouin-viscosity relation. The Brillouin line parameters of the egg white sample agree well with the branch of the water-BSA solution, as could be expected. Points of the cell cytosol are located closely to the data of the 10 wt % lysozyme solution. Various Brillouin-viscosity relations evidence that molecular structure plays a significant role for the interrelation between zero-frequency macroscopic viscosity and short-range GHz viscoelastic properties.

In this respect, the data presented in Fig. 3 have an impact on experimental techniques, which connect the cell cytosol viscosity with a local probe behavior, e.g., fluorescence molecular rotors [27]. Such experimental techniques need the calibration to find the viscosity value from the local probe parameter. Usually, solutions like water-glycerol or methanol-glycerol are used for the calibration [28–30]. However, Fig. 3(a) evidences that the relation between the high-frequency and zero-frequency viscosities is different for different fluids and, therefore, this method of calibration should lead to significant errors. At the same zero-frequency viscosity, but in different surroundings, the local probes should obey different parameters. Our outcome is that aqueous protein solutions are a better choice for the calibration in investigations of the cell cytosol viscosity.

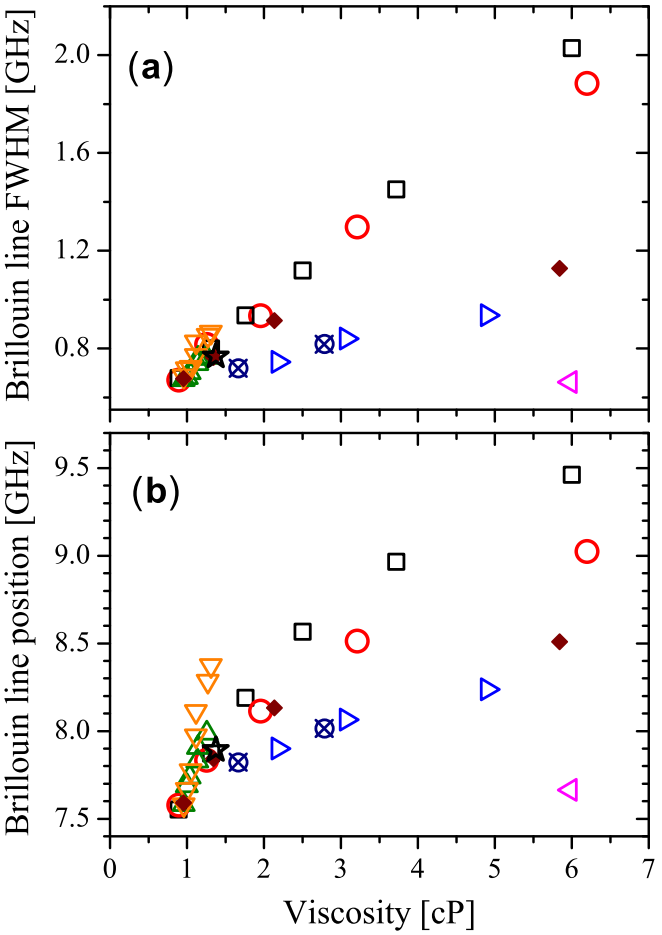

FIG. 3. Brillouin linewidth (a) and line frequency (b) of biorelevant aqueous solutions versus viscosity of nonaqueous components: glycine (down triangles), triglycine (up triangles), glycerol (squares), sucrose (circles), lysozyme (diamonds), BSA (right triangles), gelatin (left triangles). Crossed circles and star correspond to egg white and cell cytosol, respectively.

IV. CONCLUSIONS

In the present work, we found that for the majority of the biorelevant molecules studied, the concentration dependence of the Brillouin line frequency follows a universal function up to ~40 wt %. This means that local mechanical properties of cells and tissues found by Brillouin spectroscopy can be described in terms of water content. A simple approach of a biphasic substance and the same stress conditions provides an excellent description of the experimental data. On the other hand, relations between the macroscopic viscosity and the Brillouin peak parameters are different for different solutes. Thus, the accuracy of the local characterization of the zero-frequency viscosity by Brillouin spectroscopy depends on the prior knowledge about the chemical composition. The relation between the Brillouin line frequency and the zero-frequency

viscosity in the cell cytosol and egg white correspond well to the aqueous protein solutions of lysozyme and BSA, respectively, while it differs significantly from the glycerol and sucrose solutions. The last result is important for the correct choice of reference solutions for indirect experimental determinations of the cellular viscosity.

ACKNOWLEDGMENTS

This work was supported by State Assignment No. AAAA-A17-117052410033-9. Some parts of the experiments were performed in the multiple-access center "High-resolution spectroscopy of gases and condensed matter" in IA&E SBRAS, Novosibirsk, Russia.

APPENDIX: BIPHASIC MODEL

The biphasic model evaluates properties of a two-component material from parameters of the constituting components. In the case of the same stress condition, the constituting components can be represented by layers when the elastic response is considered for the external force applied along the layer normal (inset in Fig. 4). For a linear response, multiple intermittent layers composed of two different components are equivalent to two layers, as shown in the inset of Fig. 4. The ratio of the layer thickness is equal to the volume ratio of the components. Evaluation of the deformation from the elastic modulus of the components provides an effective elastic modulus of the two-component material M_{eff}, with which the aqueous solution is associated in the present work, Eq. (3). In this equation a solute and water are the components in the biphasic model. The volume fractions of the components are involved in Eq. (3). Denoting the solute density as ρ_s, the water density as ρ_W, and the solution density as ρ_{eff}, Eq. (3) corresponds to

$$\frac{1}{\rho_{\text{eff}} u_{\text{eff}}^2} = \frac{1-x}{\rho_W u_W^2} + \frac{x}{\rho_s u_s^2}, \tag{A1}$$

where x is the solute volume fraction; u_W, u_S, and u_{eff} are the sound velocities of water, solute, and solution, respectively.

The volume fractions are converted to the weight fractions via

$$x_m = x\rho_s/\rho_{\text{eff}}, \quad 1 - x_m = (1-x)\rho_W/\rho_{\text{eff}}. \tag{A2}$$

The sound velocity of the solution is found from Eqs. (A1) and (A2) as

$$u_{\text{eff}} = u_w \frac{\rho_W}{\rho_{\text{eff}}} \frac{1}{\sqrt{1 - x_m + x_m(\rho_W/\rho_s)^2(u_W/u_s)^2}}. \tag{A3}$$

Taking into account Eq. (1), the Brillouin frequency of the solution ν_b^{eff} is related to the water Brillouin peak frequency ν_b^W as

$$\nu_b^{\text{eff}} = \nu_b^W \frac{n_{\text{eff}}\rho_W}{n_W \rho_{\text{eff}}} \frac{1}{\sqrt{1 - x_m + x_m(\rho_W/\rho_s)^2(u_W/u_s)^2}}, \tag{A4}$$

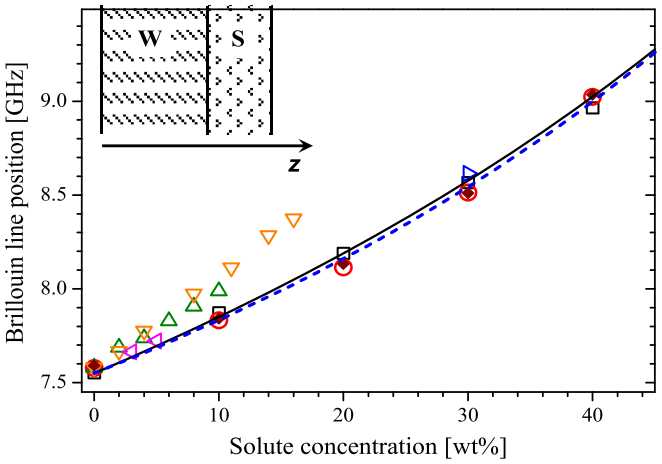

FIG. 4. Brillouin line frequency of the biorelevant aqueous solutions versus concentration of nonaqueous components. Symbols are the same as in Fig. 2. The solid line is the prediction from Eq. (4) and the dashed line is the prediction from Eq. (A8). The inset represents the geometry of the biphasic model.

where n_W and n_{eff} are the refractive indexes of water and the solution, respectively.

The two-component material in the inset of Fig. 4 corresponds to the next expression for ρ_{eff}:

$$\frac{1}{\rho_{\text{eff}}} = \frac{x_m}{\rho_s} + \frac{1-x_m}{\rho_W}. \tag{A5}$$

Effective refractive index n_{eff} can be calculated by summing the phase advances along the z axis of the material (the inset of Fig. 4):

$$n_{\text{eff}} = xn_s + (1-x)n_W. \tag{A6}$$

Using Eq. (A2) for replacing x by x_m in Eq. (A6) and Eq. (A5) for ρ_{eff}, the solution refractive index is written as

$$n_{\text{eff}} = \frac{n_s x_m \rho_W + n_W(1-x_m)\rho_s}{x_m\rho_W + (1-x_m)\rho_s}. \tag{A7}$$

Using Eqs. (A5) and (A7), Eq. (A4) can be rewritten as

$$\nu_b^{\text{eff}} = \nu_b^W \frac{1 - x_m + x_m(n_s/n_W)(\rho_W/\rho_s)}{\sqrt{1 - x_m + x_m(\rho_W/\rho_s)^2(u_W/u_s)^2}}. \tag{A8}$$

A prediction from Eq. (A8) for the solute concentration dependence of the Brillouin frequency is shown in Fig. 4. This evaluation uses the following water parameters: $n_W = 1.333$, $\rho_W = 1\,\text{g/cm}^3$, $u_W = 1.5$ km/s. For the solute parameters we take the values which are typical for organic and polymer glasses: $n_s = 1.5$, $\rho_s = 1.2\,\text{g/cm}^3$, $u_s = 3$ km/s. Figure 4 shows that taking into account the variations in the solution density and refractive index does not change the general trend coming from the simple consideration for Eq. (4).

[1] G. Scarcelli, W. J. Polacheck, H. T. Nia, K. Patel, A. J. Grodzinsky, R. D. Kamm, and S. H. Yun, Noncontact three-dimensional mapping of intracellular hydro-mechanical properties by brillouin microscopy, Nat. Methods **12**, 1132 (2015).

[2] G. Antonacci and S. Braakman, Biomechanics of subcellular structures by non-invasive brillouin microscopy, Sci. Rep. **6**, 37217 (2016).

[3] Z. Meng, S. C. B. Lopez, K. E. Meissner, and V. V. Yakovlev, Subcellular measurements of mechanical and chemical properties using dual Raman-Brillouin microspectroscopy, J. Biophotonics **9**, 201 (2016).

[4] K. Elsayad, S. Werner, M. Gallemí, J. Kong, E. R. S. Guajardo, L. Zhang, Y. Jaillais, T. Greb, and Y. Belkhadir, Mapping the subcellular mechanical properties of live cells in tissues with fluorescence emission-Brillouin imaging, Sci. Signal **9**, rs5 (2016).

[5] S. Mattana, M. Mattarelli, L. Urbanelli, K. Sagini, C. Emiliani, M. D. Serra, D. Fioretto, and S. Caponi, Non-contact mechanical and chemical analysis of single living cells by microspectroscopic techniques, Light: Sci. Appl. **7**, 17139 (2018).

[6] G. Antonacci, V. de Turris, A. Rosa, and G. Ruocco, Background-deflection Brillouin microscopy reveals altered biomechanics of intracellular stress granules by ALS protein FUS, Commun. Biol. **1**, 139 (2018).

[7] J. Zhang, A. Fiore, S.-H. Yun, H. Kim, and G. Scarcelli, Line-scanning Brillouin microscopy for rapid non-invasive mechanical imaging, Sci. Rep. **6**, 35398 (2016).

[8] F. Scarponi, S. Mattana, S. Corezzi, S. Caponi, L. Comez, P. Sassi, A. Morresi, M. Paolantoni, L. Urbanelli, C. Emiliani, L. Roscini, L. Corte, G. Cardinali, F. Palombo, J. R. Sandercock, and D. Fioretto, High-Performance Versatile Setup for Simultaneous Brillouin-Raman Microspectroscopy, Phys. Rev. X **7**, 031015 (2017).

[9] Z. Meng, A. J. Traverso, C. W. Ballmann, M. A. Troyanova-Wood, and V. V. Yakovlev, Seeing cells in a new light: A renaissance of Brillouin spectroscopy, Adv. Opt. Photonics **8**, 301 (2016).

[10] G. Scarcelli and S. H. Yun, Confocal Brillouin microscopy for three-dimensional mechanical imaging, Nat. Photonics **2**, 39 (2008).

[11] G. Antonacci, R. M. Pedrigi, A. Kondiboyina, V. V. Mehta, R. de Silva, C. Paterson, R. Krams, and P. Török, Quantification of plaque stiffness by Brillouin microscopy in experimental thin cap fibroatheroma, J. R. Soc., Interface **12**, 20150843 (2015).

[12] D. Schneider, N. Gomopoulos, C. Y. Koh, S. Papadopoulos, F. Kremer, E. L. Thomas, and G. Fytas, Nonlinear control of high-frequency phonons in spider silk, Nat. Mater. **15**, 1079 (2016).

[13] F. Palombo, M. Madami, D. Fioretto, J. Nallala, H. Barr, A. David, and N. Stone, Chemico-mechanical imaging of Barrett's oesophagus, J. Biophotonics **9**, 694 (2016).

[14] S. Mattana, M. A. Cardinali, S. Caponi, D. C. Pierantoni, L. Corte, L. Roscini, G. Cardinali, and D. Fioretto, High-contrast Brillouin and Raman micro-spectroscopy for simultaneous mechanical and chemical investigation of microbial biofilms, Biophys. Chem. **229**, 123 (2017).

[15] J. Zhang, X. A. Nou, H. Kim, and G. Scarcelli, Brillouin flow cytometry for label-free mechanical phenotyping of the nucleus, Lab Chip **17**, 663 (2017).

[16] M. Troyanova-Wood, C. Gobbell, Z. Meng, A. A. Gashev, and V. V. Yakovlev, Optical assessment of changes in mechanical and chemical properties of adipose tissue in diet-induced obese rats, J. Biophotonics **10**, 1694 (2017).

[17] I. P. Weber, S. H. Yun, G. Scarcelli, and K. Franze, The role of cell body density in ruminant retina mechanics assessed by atomic force and Brillouin microscopy, Phys. Biol. **14**, 065006 (2017).

[18] P. Shao, T. G. Seiler, A. M. Eltony, A. Ramier, S. J. J. Kwok, G. Scarcelli, R. Pineda II, and S.-H. Yun, Effect of corneal hydration on Brillouin microscopy in vivo, Invest. Ophthalmol. Visual Sci. **59**, 3020 (2018).

[19] R. Schlüssler, S. Möllmert, S. Abuhattum, G. Cojoc, P. Müller, K. Kim, C. Möckel, C. Zimmermann, J. Czarske, and J. Guck, Mechanical mapping of spinal cord growth and repair in living zebrafish larvae by Brillouin imaging, Biophys. J. **115**, 911 (2018).

[20] P. M. Chaikin and T. C. Lubensky, *Principles of Condensed Matter Physics* (Cambridge University Press, Cambridge, 2000).

[21] J. R. Sandercock, Operator manual for tandem interferometer (unpublished).

[22] M. Mijaković, B. Kežić, L. Zoranić, A. Asenbaum, C. Pruner, E. Wilhelm, and A. Perera, Ethanol-water mixtures: Ultrasonics, Brillouin scattering and molecular dynamics, J. Mol. Liq. **164**, 66 (2011).

[23] M. F. Ashby, *Material Selection in Mechanical Design* (Elsevier, Amsterdam, 2011).

[24] A. P. Sokolov, J. Hurst, and D. Quitmann, Dynamics of supercooled water: Mode-coupling approach, Phys. Rev. B **51**, 12865(R) (1995).

[25] S. Perticaroli, L. Comez, P. Sassi, M. Paolantoni, S. Corezzi, S. Caponi, A. Morresi, and D. Fioretto, Hydration and aggregation of lysozyme by extended frequency range depolarized light scattering, J. Non-Cryst. Solids **407**, 472 (2015).

[26] P.-J. Wu, I. V. Kabakova, J. W. Ruberti, J. M. Sherwood, I. E. Dunlop, C. Paterson, P. Török, and D. R. Overby, Water content, not stiffness, dominates Brillouin spectroscopy measurements in hydrated materials, Nat. Methods **15**, 561 (2018).

[27] M. K. Kuimova, Mapping viscosity in cells using molecular rotors, Phys. Chem. Chem. Phys. **14**, 12671 (2012).

[28] J. A. Levitt, M. K. Kuimova, G. Yahioglu, P. H. Chung, K. Suhling, and D. Phillips, Membrane-bound molecular rotors measure viscosity in live cells via fluorescence lifetime imaging, J. Phys. Chem. C **113**, 11634 (2009).

[29] J. E. Chambers, M. Kubánková, R. G. Huber, I. López-Duarte, E. Avezov, P. J. Bond, S. J. Marciniak, and M. K. Kuimova, An optical technique for mapping microviscosity dynamics in cellular organelles, ACS Nano **12**, 4398 (2018).

[30] A. Vyšniauskas, I. López-Duarte, N. Duchemin, T.-T. Vu, Y. Wu, E. M. Budynina, Y. A. Volkova, E. P. Cabrera, D. A. Ramírez-Ornelas, and M. K. Kuimova, Exploring viscosity, polarity and temperature sensitivity of BODIPY-based molecular rotors, Phys. Chem. Chem. Phys. **19**, 25252 (2012).